Journal of Chromatography A, 1225 (2012) 79–90

Contents lists available at SciVerse ScienceDirect

Journal of Chromatography A

journal homepage: www.elsevier.com/locate/chroma

Measurement of the eddy dispersion term in chromatographic columns: III. Application to new prototypes of 4.6 mm I.D. monolithic columns

Fabrice Gritti, Georges Guiochon*

Department of Chemistry, University of Tennessee, Knoxville, TN, 37996-1600, USA

ARTICLE INFO

Article history:
Received 9 November 2011
Received in revised form
14 December 2011
Accepted 15 December 2011
Available online 27 December 2011

Keywords:
Column technology
Mass transfer mechanism
HETP
Monolithic columns
Eddy diffusion
Trans-column effect

ABSTRACT

We investigated the mass transfer mechanism in four research prototypes of silica monolithic columns of the second generation provided by their manufacturer (Merck KGaA, Darmstadt, Germany). The heights equivalent to a theoretical plate (HETP) of these columns were measured. The different contributions to the total HETP (longitudinal diffusion term B/u_S, skeleton/eluent mass transfer resistance term Cu_S, and eddy diffusion term A) were determined experimentally for a non-retained (uracil) and for a retained (naphthalene) compound. We used the peak parking method to determine the longitudinal diffusion term, a recently developed accurate model of effective diffusion in silica monolithic structures to determine the skeleton/eluent mass transfer resistance term, and an accurate method of measurement of the total column HETP to determine the eddy diffusion term. The results show that the minimum plate heights of these monolithic column prototypes range between 6 and 7 μm for retained analytes, three times lower than those observed for monolithic columns of the first generation. A detailed analysis of the eddy diffusion term demonstrates that the improvement observed in the column efficiency is explained in part by the 40% reduction of the domain size (which provides thinner half-height peak width) but mostly by a two-fold decrease of the radial velocity bias across the silica rods (which provides more symmetrical peaks). Yet, the rods in these columns exhibit a residual radial heterogeneity leading to a minimum HETP of only 10 μm for non-retained compounds.

1. Introduction

Initially, silica monolithic rods gained much attention among chromatographers, due to their exceptionally high permeability [1–4] and to the possibility to independently adjust the average sizes of their macropores (through which flows the convective stream of mobile phase) and mesopores (the surface of which provides the retention of analytes). Chromolith™ silica monolithic columns were first commercialized in 2000, by Merck (Darmstadt, Germany). They had 2 μm macropores and 130 Å mesopores. The average size of their silica porous skeletons (called porons) was 1.3 μm. Although similar efforts were made at the same time to develop monolithic columns made of crosslinked polymers [5–7], the results were not as commercially successful.

Chromolith™ columns looked promising at a time when columns packed with 5 μm fully porous particles dominated the column market. Their specific permeability was three times larger than that of columns packed with 5 μm particles [8]. They also benefited from a fast solid/liquid mass transfer, due to the small size of their porons [9,10] and from a large sample capacity per unit adsorbent volume [11,12]. Their efficiency measured by the conventional methods based on the half-height peak width was equivalent to that of columns packed with 4 μm particles [10,13]. Yet, after a decade of investigations of their performance, these columns have not achieved the successful commercialization that was originally expected [14]. This resulted from two factors that had not been anticipated. First, accurate measurements of their efficiency [15,16] show them not to be more efficient than columns packed with 9 μm particles. This is due to the significant tailing of the elution peaks that they provide, itself caused by a structural feature inherent to their process of fabrication: the silica monolithic columns of the first generation are radially heterogeneous [17–19]. More importantly still, they soon had to face the competition of columns packed with new brands of particles, the sub-2 μm fully porous particles, which appeared in 2004 [20] and the sub-3 μm core–shell particles [21–25], which appeared in 2007 and are the modern avatar of the pellicular particles of the 1970s [26–29].

The chromatographic performance of the silica monolithic rods from the first generation suffers today from four limitations: (1) a relatively large trans-column velocity bias, about 3–4% for the 10 mm I.D. rods [18] and 2% for the 4.6 mm I.D. rods [19]; (2) a large domain size of 3.3 μm; (3) a mediocre distribution/collection frits at both ends of the column; and (4) the use of a polyether ether ketone (PEEK) clad, with restricts the maximum operating

* Corresponding author. Tel.: +1 8659740733; fax: +1 8659742667.
E-mail address: guiochon@utk.edu (G. Guiochon).

0021-9673/$ – see front matter © 2011 Elsevier B.V. All rights reserved.
doi:10.1016/j.chroma.2011.12.055

pressure to 200 bar and the use of long monolithic columns in fast chromatography. A recent investigation of the mass transfer mechanisms in 4.6 mm × 100 mm silica monolithic columns confirmed that the largest contribution (more than 95% at high flow rates) to their HETP is the eddy diffusion term of their van Deemter equation [30]. In the same time, a reconstruction of the structure of the homogeneous center zone of a 100 μm capillary monolith and the calculation of the rate of the convective-diffusive mass transfer process [31–33] showed that their low efficiency at high flow rates is not due to high trans-throughpore or short-range inter-throughpore eddy diffusion terms. Actually, the sum of the HETP terms associated to mass transfer resistances across a few throughpore diameters and along the frits/endfittings at the column ends does not exceed 4 μm. This underlines the need to develop more uniform silica structures and to design better frit/endfittings systems.

All these limitations motivated academic and industrial laboratories to prepare more radially homogeneous silica structures with smaller domain sizes and to improve frit/endfitting assemblies and the cohesion between the monolith and its cladding material. Merck Millipore (MM) (Darmstadt, Germany) and Kyoto Monotech (Kyoto, Japan) recently released column prototypes with domain sizes close to 2 μm. The Kyoto Monotech columns have dimensions of 2.3 mm × 50 mm and 3.2 mm × 50 mm. They have new frit designs and cladding material. These new columns can deliver maximum efficiencies (corrected for the extra-column band broadening contributions) and permeabilities that are equivalent to those of columns packed with 2 μm and 4 μm particles, respectively [34]. However, these columns cannot withstand inlet pressures larger than 200 bar. The Merck second generation columns are 4.6 mm × 100 mm silica rods and could also, potentially, compete with the latest particulate column technologies.

The goal of this work was to characterize and evaluate the kinetic performance of four new prototype monolithic columns (4.6 mm × 100 mm) provided by Merck Millipore. We applied the same non-invasive protocol [35,36] as already used to assess the kinetic performances of columns packed with core–shell particles [37–39], of the first generation of monolithic columns [30], and of a series of new prototype monolithic columns released by Kyoto Monotech [34]. The overall HETP is derived from accurate values of the moments of the elution band profiles obtained by numerical integration [15,16]. The external porosity of the silica monolith is measured from inverse size exclusion chromatography (ISEC) [40]. The longitudinal diffusion coefficient of the van Deemter equation (or *B* term) is given by peak parking experiments [41–43]. The trans-skeleton mass transfer resistance (*Cu* term) is obtained from the same peak parking data, using a recently validated semi-empirical model of effective diffusion in silica monolithic structures [44,45]. Finally, the residual radial structural heterogeneity is estimated on the basis of the measurement of the trans-throughpore and short-range inter-throughpores eddy diffusion terms in homogenous capillary monolithic columns taken from the recent literature [31].

2. Theory

2.1. HETP equation for monolithic columns

The general HETP equation is the sum of three independent contributions [46] that account, respectively, for (1) the longitudinal diffusion of the analyte during its migration along the column ($H_{Long.}$); (2) eddy diffusion due to all the sources of velocity biases taking place in the column at different scales, from the inter skeleton to the rod diameter lengths, across and along the column (H_{Eddy}); and (3) the resistance to mass transfer by diffusion through the porous skeleton and between the eluent streamlets and the stagnant mesoporous volumes ($H_{Skel.}$). Accordingly, the general HETP is written:

$$H = H_{Long.} + H_{Eddy} + H_{Skel.} \tag{1}$$

All necessary theoretical and technical details regarding the determination of these HETP terms in a silica monolithic column can be found in references [34,47,36]. The next sections summarized the equations for each HETP term.

2.2. Determination of the individual HETP term

2.2.1. Longitudinal diffusion HETP term

The longitudinal diffusion term $H_{Long.}$ is written [36]:

$$H_{Long.}(u_S) = \frac{B}{u_S} = 2\epsilon_e(1+k_1)\frac{D_{eff}}{u_S} = (1+k_1)\epsilon_e\frac{\Delta\sigma^2_{PP}}{\Delta t_p}\frac{u^2_{R,PP}}{u_S} \tag{2}$$

where B is the longitudinal diffusion coefficient, D_{eff} is the effective diffusion coefficient along the monolithic column, $\Delta\sigma^2_{PP}$ is the variance increment observed for an increment Δt_p of the peak parking time, $u_{R,PP}$ is the migration linear velocity of the analyte in the peak parking experiments, u_S is the superficial linear velocity of the eluent, k_1 is the zone retention factor, and ϵ_e is the external porosity of the monolithic column. By definition, k_1 is equal to:

$$k_1 = \frac{1-\epsilon_e}{\epsilon_e}[\epsilon_p + (1-\epsilon_p)K] \tag{3}$$

where K is the equilibrium constant of the analyte between the stationary phase and the bulk mobile phase and ϵ_p is the internal porosity of the porons or volume fraction of the mesopores in the skeleton volume.

2.2.2. The liquid/skeleton resistance mass transfer term

The trans-skeleton mass transfer resistance term, $H_{Skel.}$, is given by [9]:

$$H_{Skel.} = \frac{1}{16}\frac{1}{1-\epsilon_e}\left(\frac{k_1}{1+k_1}\right)^2\frac{d^2_{Skel.}}{D_{Skel.}}u_S = C_{Skel.}u_S \tag{4}$$

where $d_{Skel.}$ is the diameter of the cylindrical skeleton, which was derived from the estimate of the average throughpore diameter $d_{Throughpore}$ [48]:

$$d^2_{Throughpore} = \frac{k_0 K_G(1-\epsilon_e)^2}{\epsilon_e^3} \tag{5}$$

where the constant K_G was measured for the reference monolithic columns and is 193. Finally, the diameter of the porous elements of the skeletons can be estimated by assuming cylindrical skeleton and throughpore cross-section area:

$$d_{Skel.} = d_{Throughpore}\sqrt{\frac{1-\epsilon_e}{\epsilon_e}} \tag{6}$$

The diffusion coefficient $D_{Skel.}$ was estimated using a recently validated time-averaged model of effective diffusion in silica monolithic columns [34]:

$$D_{eff} = \frac{\gamma_e + ((1-\epsilon_e)/\epsilon_e)\Omega}{1+k_1}D_m \tag{7}$$

where D_{eff} is the experimental effective diffusion coefficient provided by the peak parking method, Ω is the ratio of the sample diffusivity in the porous adsorbent, $D_{Skel.}$, and the bulk diffusion coefficient, D_m. It is lower than unity for non-retained species because their diffusion in the mesoporous volume is restricted; it is usually above unity for retained compounds in RPLC, due to the additional contribution of surface diffusion to the total sample diffusivity [49,50]. γ_e is the external obstruction factor and can be

expressed as a function of the external porosity for a monolithic column by [36]:

$$\gamma_e = \frac{0.89}{2 - 1.11\epsilon_e} \quad (8)$$

For instance, for $\epsilon_e = 0.70$, γ_e is equal to 0.73, a value which coincides with the one obtained by morphology reconstruction and mass transfer calculations in silica monolithic structures [31].

Due to surface diffusion, the effective diffusion coefficient, D_{eff}, of retained compounds in RPLC is comparable to that of non-retained analytes, despite their stronger adsorption onto the stationary phase [51]. Their longer residence time in the column permits a more efficient relaxation of the radial concentration gradients.

2.2.3. The total eddy diffusion term

The eddy diffusion term is obtained by subtracting the longitudinal diffusion and the liquid/skeleton mass transfer resistance terms from the measured value of the overall HETP:

$$H_{Eddy} = H - H_{Long.} - H_{Skel.} \quad (9)$$

The eddy diffusion term itself is the sum of four main contributions including the impact of the trans-throughpore ($H_{Throughpore}$), the short-range inter-throughpore (H_{Short}), the trans-rod velocity biases ($H_{Trans\text{-}rod}$), and the frit/endfitting assemblies (H_{Frit}) [30,31]:

$$H_{Eddy} = H_{Throughpore} + H_{Short} + H_{Trans\text{-}rod} + H_{Frit} \quad (10)$$

The HETP terms $H_{Throughpore}$ and H_{Short} could be directly determined if the radial structure of the silica monolith was homogeneous, which it is not. Instead, it is obtained by morphology reconstruction, using confocal laser scanning microscopy (CLSM), and by calculation of the mass transfer kinetics in the center zone of a commercial 100 μm × 600 mm monolithic column with a nominal macropore size of 2 μm and a nominal skeleton thickness of 1 μm [31]. The central zone was shown to be homogeneous. These terms are written:

$$H_{Throughpore} = 0.133\frac{u_S d_{Skel.}^2}{D_m} \quad (11)$$

and

$$H_{Short} = 1.641\frac{u_S d_{Skel.}^2}{D_m}\frac{1}{1 + 1.154(u_S d_{Skel.}/D_m)} \quad (12)$$

The remaining eddy diffusion term, $H_{Trans\text{-}rod/Frit} = H_{Trans\text{-}rod} + H_{Frit}$, results from a complex combination of the radial velocity distribution, the average radial dispersion coefficient, and the band broadening contributions of the inlet and outlet connections, which distribute the in-going stream across the inlet cross-section of the column and collect the out-going streamlets. This term is unknown but can be estimated by subtracting the first two terms from the overall eddy diffusion term or:

$$H_{Trans\text{-}rod/Frit} = H_{Eddy} - H_{Throughpore} - H_{Short} \quad (13)$$

Finally, the HETP contributions of the frit/endfitting assemblies should be subtracted from $H_{Trans\text{-}rod/Frit}$ in order to extract the following HETP term, $H_{Trans\text{-}rod}$, caused by the sole radial velocity gradients across the silica rod:

$$H_{Trans\text{-}rod} = H_{Trans\text{-}rod/Frit} - H_{Frit} \quad (14)$$

2.3. Determination of the true chromatographic HETP

The systematic protocol applied to determine accurate values of the HETP is detailed elsewhere [16,34]. The same protocol was applied in this work as in part II. In part I (first generation of monolithic columns) [30], the same measurements were performed manually, one peak after the other. Both methods provide exactly the same results, within less than 0.1% (first moment) and 0.5% (second moment) but the time required with the new method is much reduced.

In this work, the widths of the integration interval were set at $n = 5$ and $n = 4$ for the non-retained (uracil) and the retained (naphthalene) compounds, respectively. The peak apex was positioned at precise fractions $p = 0.375$ (uracil) and $p = 0.450$ (naphthalene) in order to adjust for the differences in degrees of peak tailing. This method guarantees that accurate values of the first, second, and third moments will be obtained, with relative errors of 0.1, 2, and 10% for strongly tailing peaks, respectively [52]. Accordingly, 5–10% precise HETP values corrected for the extra-column contributions can be obtained, depending on the relative contribution of the extra-column peak variance to the total peak variance [15]. Illustration of the calculation of the first and second central moments is given in Fig. 1A and B. The flow rate was set at 2.5 mL/min on the prototype column UM402.835. The asymmetry of the peaks eluted from these prototype columns depends on the analyte retention.

The relative standard errors (accuracy) made on the corrected HETP are between 1.2% (if the extra-column contributions are negligible) and 3% (when the largest extra-column contribution accounts for 7% of the total peak variance).

3. Experimental

3.1. Chemicals

The mobile phase was a mixture of acetonitrile and water (55/45, v/v). Tetrahydrofuran was used as the eluent for the inverse size-exclusion chromatography (ISEC) measurements. All these solvents were HPLC grade from Fisher Scientific (Fair Lawn, NJ, USA). The mobile phases were filtered before use on a surfactant-free cellulose acetate filter membrane, 0.2 μm pore size (Suwannee, GA, USA). Eleven polystyrene standards (MW = 590, 1100, 3680, 6400, 13,200, 31,600, 90,000, 171,000, 560,900, 900,000, and 1,877,000) were used to acquire ISEC data. They were purchased from Phenomenex (Torrance, CA, USA). The low molecular weight compounds used in this work were uracil and naphthalene, with a minimum purity of 99% (Fisher Scientific).

3.2. Apparatus

The 1290 Infinity HPLC system (Agilent Technologies, Waldbroen, Germany) liquid chromatograph used in this work includes a 1290 Infinity Binary Pump with Solvent Selection Valves and a programmable auto-sampler. The injection volume was set at 1.0 μL and was drawn into one end of the 20 μL injection loop. The instrument is equipped with a two-compartment oven and a multi-diode array UV–vis detection system. The system is controlled by the Chemstation software. The sample trajectory in the equipment involves the successive passage of its band through

- A 20 μL injection loop attached to the injection needle. The design of the injection system is such that the volume of sample drawn into the loop is the volume of sample injected into the column.
- A small volume needle seat capillary (115 μm I.D., 100 mm long), ≃ 1.0 μL, located between the injection needle and the injection valve. The total volume of the grooves and connection ports in the valve is around 1.2 μL.
- Two 130 μm × 250 mm long Viper capillary tubes placed, one before, the second after the column. They were offered by the manufacturer (Dionex, Germering, Germany). Their total volume is 6.6 μL.

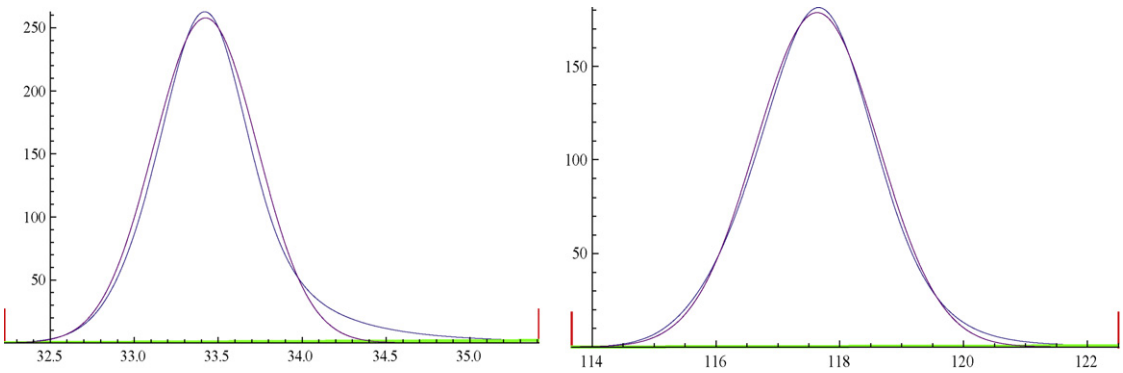

Fig. 1. Measurements of the first and second central moments of uracil (left) and naphthalene (right) eluted from a 4.6 mm × 100 mm silica monolithic column (UM402.835) at a flow rate of 2.5 mL/min. T = 297.3 K. The ordinate units are absorbance (mAU); on the x-axis, they are time (s). The experimental peak profile is the solid blue line. The linear baseline correction is shown by the solid green line. The boundaries and the position of the integration interval are delimited by the left and right red vertical segments. The best fit of the experimental peak profile to a Gaussian curve is shown as the solid purple curve. (For interpretation of the references to color in this figure legend, the reader is referred to the web version of the article.)

- A small volume detector cell, 0.8 μL, 10 mm path.

The extrapolation to a zero flow rate of the extra-column volume measured for 1.0 μL injections of uracil and naphthalene tracers in the flow rate range between 0.10 and 1.0 mL/min provides an average extra-column volume of 11.4 μL. According to the dimensions just cited, we should expect a volume of 0.5 (injection volume) + 1.0 (needle seat capillary) + 1.2 (injection valve) + 6.6 (inlet and outlet capillaries) + 0.4 (detector cell) = 9.7 μL. Given the wide range of the specifications (± 20%) for the inner diameter of the connecting capillary tubes, these two values are in good agreement. We measured an offset time of about 0.07 s between the moments when the zero time is recorded and when the sample leaves the injection needle. Note that the extra-column peak variance measured with the Viper connector rapidly increases from 5.3 μL^2 at 0.1 mL/min to 11.5 μL^2 at 1.3 mL/min and remains nearly constant at higher flow rates up to 3.0 mL/min.

3.3. Columns

Four research silica monolith prototypes were generously offered to us by Merck Millipore (Darmstadt, Germany). All these columns have the same dimensions, 4.6 mm × 100 mm. Their physico-chemical characteristics (total, external, and internal porosities, average mesopore size, predicted ratio of poron's sample diffusivity to the bulk diffusion for a non-retained compound, average skeleton diameter, average throughpore diameter, and specific permeability) were derived in this study. They are listed in Table 1. The modified silica-C_{18} surface was fully endcapped, according to a proprietary process. The 4.6 mm × 100 mm column packed with 1.9 μm non-porous silica particles that we used for the measurement of the diffusion coefficient of uracil and naphthalene was a generous gift from Phenomenex (Torrance, CA, USA).

These new monolithic columns are representative of the average samples prepared by Merck Millipore. In contrast, in part II, the prototype monolithic columns sent to us by the manufacturer were selected among those that provide the highest plate counts.

3.4. Peak parking (PP) measurements

The PP method was used to measure the longitudinal diffusion HETP terms ($H_{Long.}(u_S)$) of the monolithic columns studied and the effective diffusivities ($D_{Skel.}$) of the samples through their porous skeleton. Details and applications of this technique can be found elsewhere [53,41,42,54,55]. In the PP experiments reported, 2 μL of a dilute sample solution (< 0.5 g/L) was injected at a low, constant flow rate of 0.30 mL/min, in order to keep the same low superficial linear velocity, e.g. a similar low pressure drop along the column during the elution. The column was eluted during the time necessary for the non-retained sample (uracil) to reach about 3/4 of the length of the column. Since the retention factors measured for naphthalene on the four monolithic columns were all around 2.5 ± 0.1, respectively, this compound was parked at about 1/5 of the lengths of these columns. When the uracil band has reached the desired position, the flow is abruptly stopped and the samples are left free to diffuse along the column, around their position, during a certain time (the parking time, t_p). This time was successively set at 1, 15, 30, 60, and 90 min. The peak variances measured as a function of the parking time are gathered in Fig. 2. They will be discussed later.

The slopes of the plots of the elution peak variances *versus* the peak parking times, $\Delta\sigma^2_{PP}/\Delta t_p$, provide a direct measure of the effective diffusion coefficients along the packed bed (D_{eff}) and an estimate of the sample diffusivity through the porous skeleton ($D_{Skel.} = \Omega D_m$), as explained in the theory Sections 2.2.1 and 2.2.2,

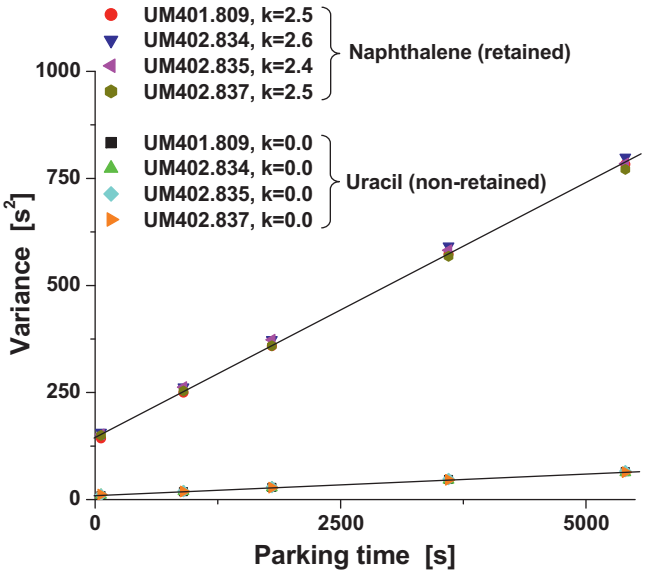

Fig. 2. Plots of the variances of the eluted band profiles recorded during the peak parking experiments *versus* the peak parking time. Four monolithic columns and two solutes (retained and non-retained) were used as indicated in the graph legend. For all columns the superficial linear velocity was fixed at 0.040 cm/s. The peak parking times were set at 1, 15, 30, 60, and 90 min. Note the column-to-column repeatability.

Table 1
Physico-chemical property of the four silica-C_{18} monolithic columns prepared by Merck Millipore measured in our lab.

Column's serial number	Column's dimension I.D. [mm] × length [mm]	Total porosity[a] (ϵ_t)	External porosity[b] (ϵ_e)	Shell porosity[c] (ϵ_p)	Average mesopore diameter[d] (d_{pore}, [Å])	Expected shell diffusivity[h] (Ω)	Average skeleton diameter[e] ($d_{Skel.}$, μm)	Average throughpore diameter[f] ($d_{throughpore}$, μm)	Permeability[g] (k_0, cm^2)
UM401.809	4.6 × 100	0.831	0.668	0.491	109	0.21	0.74	1.05	1.54×10^{-10}
UM402.834	4.6 × 100	0.821	0.661	0.472	107	0.19	0.87	1.21	1.91×10^{-10}
UM402.835	4.6 × 100	0.821	0.661	0.472	107	0.19	0.88	1.23	1.98×10^{-10}
UM402.837	4.6 × 100	0.813	0.654	0.46	108	0.19	0.91	1.26	1.91×10^{-10}

[a] Value obtained from the corrected elution volume of ethylbenzene in pure tetrahydrofuran.
[b] Value obtained from the extrapolation of the exclusion branch of the ISEC plots.
[c] Value calculated from $(\epsilon_t - \epsilon_e)/(1 - \epsilon_e)$.
[d] Value obtained from the intersection of the exclusion and intrusion branches of the ISEC plots (after C_{18} derivatization).
[e] Value estimated assuming cylindrical pore and skeleton shapes.
[f] Value obtained from the Ergun permeability law and the reference permeability of commercial Chromolith™ column ($k_0 = 7.9 \times 10^{-10}$ cm^2 and $d_{Throughpore} = 2.0$ μm).
[g] Value obtained from the corrected pressure drop measurements (eluent: CH_3CN/H_2O, 55/45, v/v).
[h] Value expected for a non-retained compound (uracil) from the present ISEC data, Mitzithras data [58], Pismen [56], and Renkin [57] correlations.

respectively. The larger slopes observed for the retained analyte are mostly explained by its larger retention factor, e.g. by its migration linear velocity along the column being smaller than that of the non-retained compound.

3.5. Measurement of the bulk diffusion coefficients D_m

The diffusion coefficients of uracil and naphthalene were measured by applying the peak parking method with a 100 mm × 4.6 mm column packed with solid, non-porous silica particles (1.9 μm). All the necessary details are given in [34]. The values of the bulk molecular diffusion coefficients of uracil and naphthalene during the HETP and PP runs of each column are listed in Tables 2 and 3 (fourth column).

3.6. HETP plots

For all columns, the same sequence of superficial linear velocities was applied. The flow rates were set at 0.10, 0.20, 0.30, 0.40, 0.60, 0.80, 1.00, 1.30, 1.50, 1.80, 2.00, 2.50, and 3.00 mL/min. The data acquisition rate was adjusted to 2.5, 5, 5, 10, 10, 20, 20, 20, 40, 40, 40, 40, 80, 80, and 80 Hz, respectively, in order to record peak profiles with a comparable number of data points (> 90) at all flow rates. 1 μL samples of the solution (concentration < 0.5 g/L) were injected into the columns and the chromatograms were recorded at the same wavelength of 265 nm. For all samples, a constant bandwidth of 4 nm was selected. The temperature was set by the laboratory air-conditioner at 296.3 ± 1 K.

3.7. ISEC experiments

The ISEC experiments were carried out with neat THF as the eluent. Twelve polystyrene standards were used, with molecular weight between 100 and 2 millions Da. This covers a wide range of molecular sizes between 4 and 950 Å. The flow rate was set at 0.30 mL/min for all columns. The external porosity was determined from the extrapolated elution volumes of the exclusion branches to a molecular radius of zero divided by the column tube volume (1.66 cm^3). The average mesopore size after C_{18} derivatization and surface endcapping was estimated from the diameter of the polystyrene standard at the intersection between the intrusion and exclusion ISEC branches. The total porosity of each column was measured from the elution time of ethyl-benzene present in all polystyrene standards. All the results are listed in Table 1.

4. Results and discussion

We discuss first the permeability of the four columns and estimates of their average throughpore and skeleton sizes. The average mesopore size was also estimated from the ISEC plots. For the sake of comparison, the first generation of monolithic columns commercialized by Merck KGaA in 2000 had an average specific permeability of 7.9×10^{-14} m^2 [8,4,14], an average throughpore size of 2 μm [13,4], an average skeleton size of 1.3 μm [13,4], and an average mesopore size of 120 Å before C_{18} derivatization [4]. Then, we report on the overall kinetic performance of these new monolithic columns for a non-retained and a retained compound, using a general experimental protocol [47,36]. Finally, we estimate the residual trans-column heterogeneity of these columns from their trans-rod eddy diffusion term measured with a non-retained compound and we compare the results obtained to those previously published for the first generation of monolithic columns [30].

4.1. Permeability of the monolithic columns

The pressure drops along the monolithic columns were measured by subtracting the system pressure drop (measured in the absence of a column) from the total pressure drop (measured in the presence of the column) at flow rates of 0.10, 0.20, 0.30, 0.40, 0.60, 0.80, 1.00, 1.30, 1.50, 1.80, 2.00, 2.50, and 3.00 mL/min. The eluent was a mixture of acetonitrile and water (55/45, v/v), the temperature was 297.1 K. The viscosity of the mobile phase was then $\eta = 0.779$ cP. It is noteworthy that, when using two 130 μm × 250 mm Viper connecting tubes, the system pressure contribution to the total pressure drop is about 30–35% at high linear velocities ($0.1 < u_S < 0.3$ cm/s). The plots of these corrected pressure drops *versus* the applied flow rates are shown in Fig. 3 for the four columns studied. The pressure drop, ΔP, is given by the general permeability equation [46]:

$$\Delta P = \frac{\eta L}{\pi R_c^2 k_0} F_v \quad (15)$$

For all the columns, the slopes of the linear plots shown in Fig. 3 were measured for $u_S < 0.1$ cm/s. These slopes provide estimates of the specific permeability, k_0, of each column, knowing its internal radius (R_c =0.23 cm). The values are 1.54, 1.91, 1.98, and 1.91 × 10^{-14} m^2 for the columns UM401.809, UM402.834, UM402.835 and UM402.837, respectively. In fact, the last three silica rods were prepared from the same batch while the first one was obtained from a gel with a different composition, which resulted in a slightly less permeable silica rod or a smaller average throughpore size for UM401.809. If we consider the last three silica rods, their

Table 2
Temperatures (T), diffusion coefficients (D_m), zone retention factor (k_1), effective diffusion coefficients (D_{eff}), ratio of the shell diffusivity to the bulk diffusion (Ω), reduced longitudinal diffusion coefficients (B), and solid–liquid mass transfer coefficient (C_p) measured for the non retained compound uracil.

Column's serial number	Column's dimension I.D. [mm] × length [mm]	T [K]	D_m [cm^2/s]	k_1	D_{eff} [cm^2/s]	Ω	B [cm^2/s]	$C_{Skel.}$ [μs]
UM401.809	4.6 × 100	295.6	1.01×10^{-5}	0.26	6.71×10^{-6}	0.26	1.13×10^{-5}	16.2
UM402.834	4.6 × 100	297.0	1.05×10^{-5}	0.20	7.08×10^{-6}	0.21	1.12×10^{-5}	17.4
UM402.835	4.6 × 100	297.3	1.06×10^{-5}	0.23	7.05×10^{-6}	0.24	1.15×10^{-5}	20.7
UM402.837	4.6 × 100	296.9	1.04×10^{-5}	0.22	7.05×10^{-6}	0.23	1.12×10^{-5}	19.9

Table 3
Same as in Table 2, except the compound, naphthalene.

Column's serial number	Column's dimension I.D. [mm] × length [mm]	T [K]	D_m [cm^2/s]	k_1	D_{eff} [cm^2/s]	Ω	B [cm^2/s]	$C_{Skel.}$ [μs]
UM401.809	4.6 × 100	295.6	1.21×10^{-5}	3.38	6.32×10^{-6}	3.19	3.90×10^{-5}	15.9
UM402.834	4.6 × 100	297.0	1.26×10^{-5}	3.42	6.39×10^{-6}	3.01	3.93×10^{-5}	21.9
UM402.835	4.6 × 100	297.3	1.27×10^{-5}	3.21	6.89×10^{-6}	3.10	3.98×10^{-5}	21.3
UM402.837	4.6 × 100	296.9	1.25×10^{-5}	3.31	6.62×10^{-6}	2.99	3.83×10^{-5}	23.8

permeabilities are exactly four times smaller than that obtained for the first generation of monolithic columns (7.9×10^{-14} m^2). This shows that their domain size is significantly smaller.

The external porosities of the monolithic columns UM401.809, UM402.834, UM402.835 and UM402.837 were derived from the ISEC plots shown in Fig. 4A–D and found to be 0.67, 0.66, 0.66, and 0.65, respectively. The total porosities measured from the elution times of ethyl-benzene in neat THF (non-retained conditions) are 0.83, 0.82, 0.82, and 0.81, respectively. Mercury porosimetry experiments provided values of the specific mesopore and macropore volumes of 0.93 mL/g and 2.48 mL/g, respectively. So, the ratio of the macroporous (external) to the total porous volume is 2.48/(2.48 + 0.93) = 0.73. The same ratio measured from the ISEC data is 0.66/0.82 = 0.80. The slight differences (+10%, ISEC/Hg-porosimetry) lies essentially in the fact that molecules of nitrogen can access a larger internal volume than the more voluminous molecules of ethyl-benzene.

From Eq. (5) with $K_G = 193$, the average throughpore sizes of columns UM401.809, UM402.834, UM402.835 and UM402.837 are 1.05, 1.21, 1.23, and 1.26 μm, respectively. According to mercury porosimetry data provided by the manufacturer, an average throughpore size of 1.16 μm was found for the silica rod

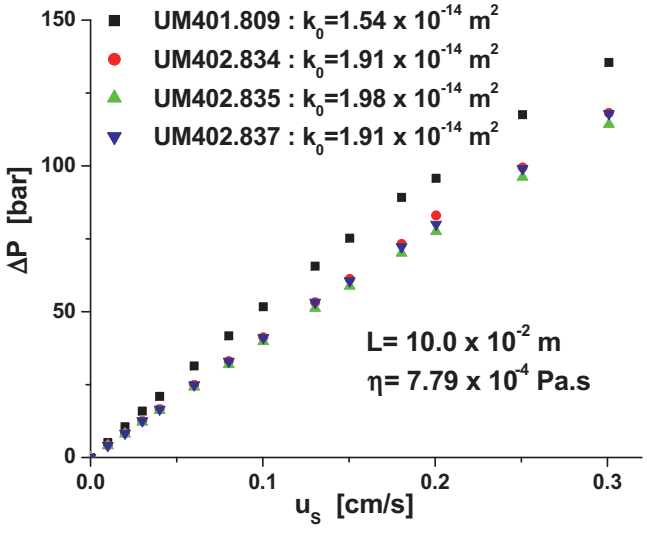

Fig. 3. Column pressure drops recorded as a function of the superficial linear velocity. k_0 is the column specific permeability.

UM401.809, in good agreement with our experimental estimates in Table 1 (ninth column).

Compared to first generation columns, the average throughpore size has decreased from 2.0 to 1.2 μm, a 40% relative decrease. Eq. (6) was used to estimate the average skeleton sizes, giving values of 0.74, 0.87, 0.88, and 0.91 μm, respectively. Thus, if we exclude the first sample, the average skeleton size has decreases from 1.3 to 0.9 μm, a relative reduction of 31%. Overall, the domain size (sum of the throughpore and the skeleton sizes) has decreased from 3.3 to 2.1 μm, a 36% relative diminution.

The intersection of the exclusion branch with the intrusion branch of the ISEC plot provides a good estimate of the average mesopore size, $\overline{d_{pore}}$, after bonding of the silica surface with C_{18} chains and the proprietary surface endcapping. Values of 109, 107, 107, and 108 ± 10 Å were found. All these data are listed in Table 1. These values are consistently smaller than those measured by low temperature nitrogen adsorption experiments (146 Å) or mercury porosimetry (141 Å) for the research sample UM401.809 before surface modifications. They will be used later for estimating the ratio, Ω, of the intra-skeleton diffusivity to the bulk molecular diffusion coefficient of a non-retained compound (uracil) [34], in combination with the Pismen correlation [56] (obstruction factor γ_p), the Renkin correlation [57] (hindrance diffusion factor, $F(\lambda_m)$), and the reference experimental data of Mitzithras [58].

4.2. Performance of the monolithic columns

Fig. 5A–D shows the plots *versus* the mobile phase flow rate of the HETPs corrected for extra-column band broadening of the four new monolithic columns studied.

As for the first generation of silica monolithic columns [30], the minimum HETP for naphthalene ($k = 2.5$) is always lower than for uracil ($k = 0$). As previously demonstrated [59,30,50,60], the larger residence times of retained compounds in the column combined with their faster diffusivity across the stationary phase permits a more efficient relaxation of the radial concentration gradients caused by the radial structure heterogeneity. Therefore, the HETP curves of naphthalene and uracil intersect at a superficial linear velocity u_S close to 0.4 mm/s. This observation confirms that the eddy diffusion of uracil is larger than that of naphthalene, despite its lower longitudinal diffusion B term. This is due to the lack of surface diffusion for the unretained uracil. Remarkably, this behavior differs from those observed with the two new silica monolithic columns prepared by Kyoto Monotech [34]. Recent kinetic investigations of these prototype columns unambiguously showed that

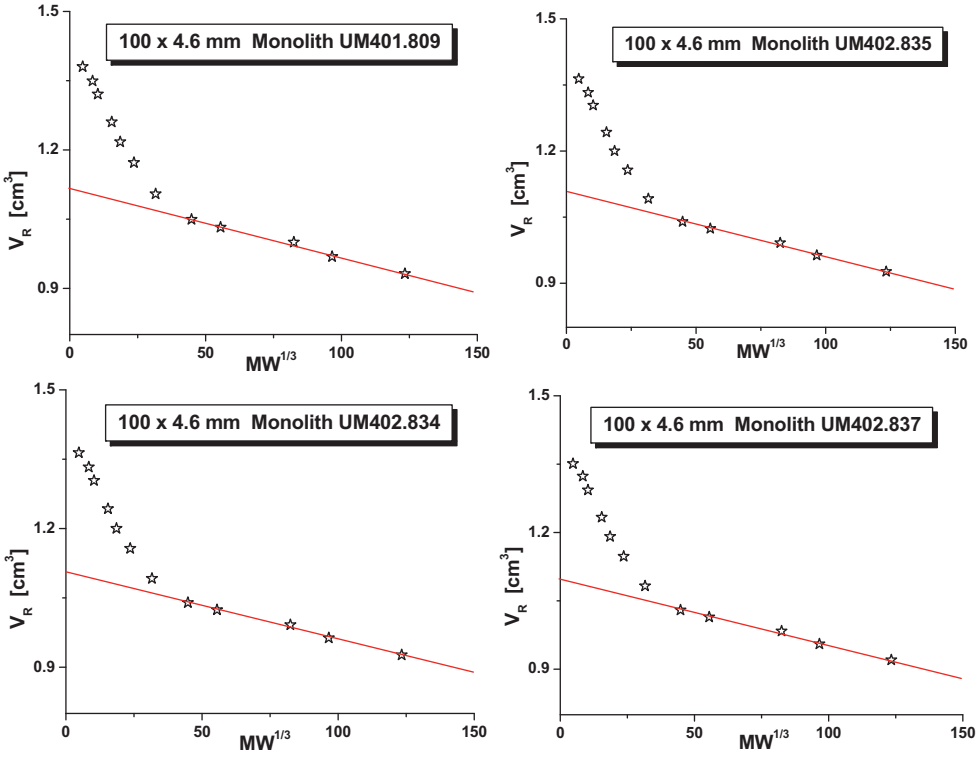

Fig. 4. ISEC plots constructed from the elution volumes of twelve polystyrene standards normalized to the column tube volume. The red solid line is the exclusion branch. The external porosity is measured at the intersection point between the solid red line and *y*-axis. (For interpretation of the references to color in this figure legend, the reader is referred to the web version of the article.)

the HETPs of uracil and naphthalene measured under the very same experimental conditions (eluent acetonitrile/water, 55/45, v/v), never intersect. The HETP curve of uracil was found below that of naphthalene at all flow velocities. On the average, the minimum HETPs of uracil and naphthalene were 4.5 and 6.5 μm, respectively. In this work, the minimum HETPs of the Merck prototype columns measured for naphthalene are 6.5 (UM401.809), 6.9 (UM402.834), 6.8 (UM402.835), and 7.0 μm (UM402.837), values comparable to

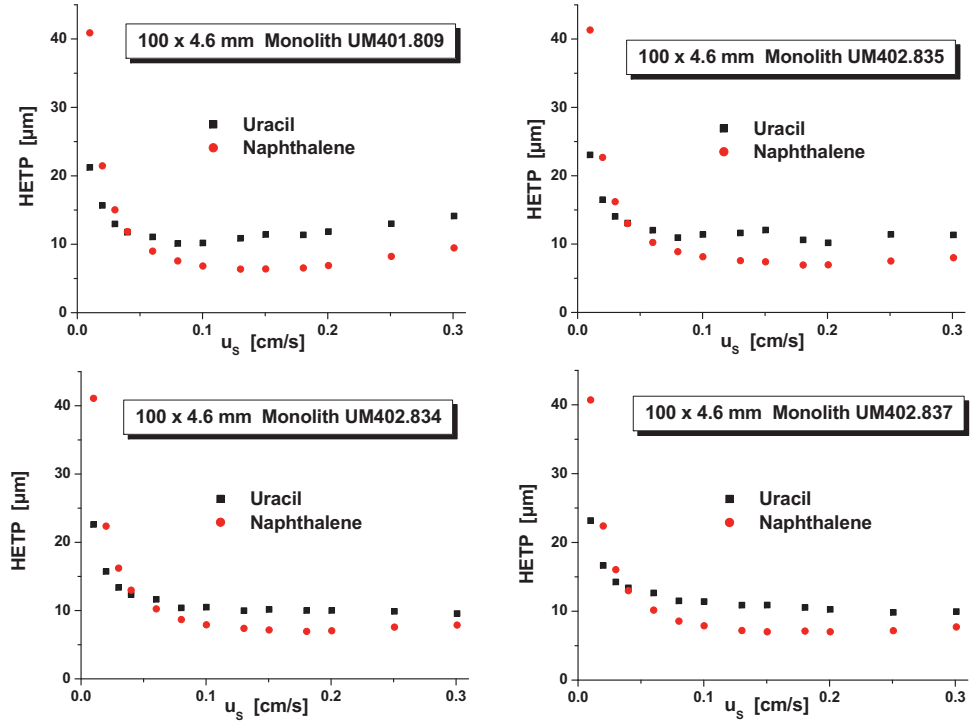

Fig. 5. Corrected HETPs of the four monolithic columns measured for a non-retained (uracil) and retained (naphthalene) compounds. The two HETP curves intersect at the same superficial linear velocity of 0.4 mm/s ($H \simeq$ 11–13 μm). The minimum HETP (6–7 μm) is observed with the retained analyte.

those previously observed with narrower and shorter monolithic columns. This is not surprising when we realize that moderately retained analytes are very forgiving to minor degrees of the radial heterogeneity of a column [60]. In contrast, the minimum HETPs of the non-retained compounds are much larger, at 10.2 (UM401.809), 9.9 (UM401.834), 10.1 (UM401.835), and 9.9 μm (UM401.837), values about twice larger than those measured with the 2.3 mm × 50 mm and 3.2 mm × 50 mm I.D. columns from Kyoto Monotech. Therefore, this suggests that the new prototype silica rods prepared by Merck (this work) are slightly less radially homogeneous than those prepared by Kyoto Monotech [34]. This makes sense because it is always more challenging to prepare wide than narrow radially homogeneous silica rods. This will be confirmed later from the measurement of the sole eddy diffusion term.

Nevertheless, since the minimum HETP of the monolithic columns of the first generation was as large as 18 μm [30], the new wide silica monolithic rods prepared by Merck Millipore provide a much lower minimum plate height, one that is similar to those of 3.5 μm conventional fully porous particles for moderately retained compounds. Most importantly, as shown in a previous section, they also have the permeability of columns packed with 4.5 μm spherical particles.

In the next sections, we report on the values of the eddy diffusion terms derived for uracil and naphthalene in the four monolithic columns, according to Eq. (9). This determination required the measurements of the longitudinal diffusion term (known from Eq. (2), the peak parking data given in Fig. 2) and the solid–liquid mass transfer resistance term. This last term depends on the analyte diffusivity through the porous skeleton (see Eq. (4)), which was estimated from the combination of the peak parking measurements with the time-averaged model of effective diffusion in a monolithic column.

4.2.1. Validation of the time-average model of effective diffusion in monolithic columns

In order to confirm previous findings regarding the accuracy of the time-averaged model to predict the experimental effective diffusion coefficient in a monolithic column [34], we consider the case of a non-retained analyte (uracil) because, for such compounds only, we can calculate with a satisfactory accuracy the ratio, Ω, of its diffusivity across the porons to its bulk molecular diffusion coefficient.

In the absence of sample adsorption, Ω is simply the product of the poron porosity, ϵ_p (measured from ISEC data), by the obstruction factor, $\gamma_p(\epsilon_p)$ (estimated from Pismen correlation [56]), and by the hindrance diffusion factor, $F(\lambda_m)$ (estimated from Renkin correlation [57]). Note that λ_m is the ratio of the analyte size (5.0 Å) to the average mesopore size, $\overline{d_{pore}}$, after C_{18} derivatization and endcapping. The average mesopore size was estimated from the intersection point between the exclusion and intrusion ISEC branches. We found $\overline{d_{pore}}$ = 109 Å (UM401.809), 107 Å (UM402.834), 107 Å (UM402.835), and 108 Å (UM402.837). The relative error made on the parameters γ_p and $F(\lambda_m)$ are typically around 30 and 10%, respectively. Additionally, the values of Ω were scaled to the reference experimental data obtained by Mitzithras [58] for a porous silica powder ($\overline{d_{pore}}$ = 108 Å, $\lambda_{m,ref}$ = 0.046) with a porosity $\epsilon_{p,ref}$ = 0.67. They measure $\gamma_{p,ref}F(\lambda_{m,ref})$ = 0.52.

Accordingly, we calculate the Ω values from:

$$\Omega = \frac{\epsilon_t - \epsilon_e}{1-\epsilon_e} 0.52 \frac{\gamma_p(\epsilon_p)}{\gamma_p(\epsilon_{p,ref})} \frac{F(\lambda_m)}{F(\lambda_{m,ref})} \quad (16)$$

These predicted values of Ω (uracil) are then 0.21, 0.19, 0.19, and 0.19 for the monolithic columns UM401.809, UM402.834, UM402.835 and UM402.837, respectively.

We also determined the Ω parameters of uracil on the four monolithic columns on the basis of the results of the peak parking measurements, using the time-averaged model of effective diffusion in binary composite media (Eq. (7)). The experimental values of Ω are the unique solution of the following equation:

$$D_{eff} = \frac{1}{2}\frac{\Delta\sigma^2_{PP}}{\Delta t_p} u^2_{R,PP} = \frac{\gamma_e + ((1-\epsilon_e)/\epsilon_e)\Omega}{1+k_1} D_m \quad (17)$$

These experimental values (see seventh row in Table 2) are 0.26, 0.21 0.24, and 0.23 for the monolithic columns UM401.809, UM401.834, UM401.835 and UM401.837, respectively. They are larger by only 23, 10, 26, and 21% than the calculated values of Ω. Therefore, they remain within the error interval (±40%), which confirms that the time-averaged model of effective diffusion is suitable to predict the accurate sample diffusivities across the porons. This model is used later to estimate the skeleton/liquid mass transfer resistance term.

4.2.2. Longitudinal diffusion

The longitudinal diffusion coefficients, $B = 2(1+k_1)D_{eff}$, are listed in the eighth column of Table 2 (uracil) and Table 3 (naphthalene). They were derived directly from the peak parking data using Eq. (2). The B coefficients of each compound are very similar and remain nearly independent of the average sizes of the macropores and porons. This indirectly confirms that the phase ratios, $F = (1-\epsilon_e)/\epsilon_e$, are very similar for all monolithic columns, as confirmed experimentally by the ISEC data in Table 1 ($0.654 < \epsilon_e < 0.668$). It is noteworthy that the B values are thrice larger for naphthalene than for uracil. This is the direct effect of surface diffusion taking place in the porons with the retained compound. The Ω values measured for naphthalene (3.1 ± 0.1) are significantly larger than those found with uracil (0.23 ± 0.03). In other words, the total diffusive flux of naphthalene molecules through the porons is mostly (≃ 90%) accounted for by the flux in the sole adsorbed state where the sample is concentrated (naphthalene is about five times more concentrated in the stationary than in the mesoporous volume). This explains why the HETP curve of naphthalene is largely above that of uracil at low flow velocities ($u_S < 0.4$ mm/s).

The difference between the B coefficient and the effective diffusion coefficient, D_{eff} in the general van Deemter equation must be underlined. The apparent diffusion of naphthalene along the column (effective diffusion does take place in an empty column tube filled only with eluent) is slowed down due to its retention (k_1) in the stationary phase. Therefore, it is not surprising to see in Tables 2 and 3 that D_{eff} for naphthalene ($\simeq 6.6 \times 10^{-6}$ cm^2/s) is comparable if not slightly smaller than for uracil ($\simeq 7.0 \times 10^{-6}$ cm^2/s). In summary, the retention (k_1) of analytes in RPLC compensates for their large diffusivity (Ω) in the stationary phase. Because retained molecules have a larger residence time in the column, the contribution of their longitudinal diffusion term to the total column HETP is obviously larger for retained than for non-retained samples [61]. More details on the fundamental differences between the coefficients B and D_{eff}, are available in several publications [36,44,45,47,49].

Obviously, the longitudinal diffusion plate height has little impact on the total plate height at high flow rates. For instance, at the maximum superficial linear velocity of 3 mm/s, the corresponding $H_{Long.}$ values are 0.4 μm (for uracil, 4%) and 1.3 μm (for naphthalene, 16%). In contrast, at the lowest velocity applied (0.1 mm/s), this contribution is maximum at 11.2 μm (for uracil, 48%) and 38.2 μm (for naphthalene, 94%).

4.2.3. Skeleton/liquid mass transfer resistance term

The poron/liquid mass transfer resistance was measured according to a protocol defined earlier [36,47] and Eq. (4). Because we deal with small molecules ($D_{Skel.} \simeq 10^{-5}$ cm^2/s) and the average skeleton size is thin ($d_{Skel.} \simeq 1$ μm), we can approximate the mean diffusion time across the porons to half a millisecond. This diffusion time

is comparable to the convective time necessary to move the band ahead by one domain size (2.1 μm) at the highest interstitial linear velocity of 0.45 cm/s. Thus, the HETP contribution of the solid/liquid mass transfer resistance term to the total HETP is nearly negligible. For instance, at this highest interstitial linear velocity, the corresponding plate heights are no larger than 0.06 μm (for uracil) and 0.07 μm (for naphthalene). As expected, mass transfer through the porons of silica monolith columns is very fast and its plate height contribution is negligible compared to the longitudinal diffusion and eddy diffusion HETP terms [62].

4.2.4. Eddy diffusion term

The eddy diffusion term of the van Deemter equation was measured according to Eq. (9). The four plots of this term *versus* the superficial linear velocity are shown in Fig. 6A–D.

Strikingly, as anticipated in the previous sections, the residual eddy diffusion term of uracil is about twice larger than that of naphthalene. It is impossible to argue about the large decrease of the eddy diffusion term of uracil from the columns of the first ($H_{Eddy} \simeq 20$ μm) to those of the second ($H_{Eddy} \simeq 10$ μm) generation prepared by Merck Millipore. However, the decrease of this term for uracil does not match that observed for this term of the retained compound, which remains high ($H_{Eddy} \simeq 5$ μm). In other words, the structure of the new monolithic column is not yet perfectly radially homogeneous.

The new monolithic columns benefit from the significant diminution of the domain size and from an improvement, still incomplete, of the radial homogeneity of the rod. Obviously, the value for the retained analytes is less sensitive to the residual radial heterogeneity of the column rod due to their large residence time and high diffusivity (ΩD_m) across the porons [60].

Preparing 4.6 mm I.D. and radially homogeneous silica rods seems to remain a challenging task. Serious progress were made by Kyoto Monotech but for narrower (2.3 and 3.2 mm I.D.) and shorter (50 mm long) rods [34]. Their eddy diffusion term for uracil was as low as that for naphthalene under the same eluent conditions. One can estimate a residual eddy diffusion term, $H_{Trans\text{-}rod/Frit}$, by subtracting the contributions of the HETP terms $H_{Throughpore}$ and H_{Short} from the overall eddy diffusion term, H_{Eddy} (see Eq. (13)). These two HETP terms were determined by morphology reconstruction of the uniform center zone of a 100 μm I.D. silica monolith and calculation of the mass transfer through this structure [31]. The numerical expressions are given by Eqs. (11) and (12). On the average, for all four columns, the residual eddy diffusion term reduces to about 8 μm for a non-retained compound and 3 μm for a moderately retained compound at high linear velocity. Likely, the residual HETP of 3 μm measured for naphthalene accounts for the band broadening (H_{Frit}) taking place along the imperfect frits and endfittings, at both ends of the column.

The residual trans-rod velocity bias can be estimated based on the general theory of flow dispersion of Giddings. The trans-rod HETP term, $H_{Trans\text{-}rod}$, is then written by [46]:

$$H_{Trans\text{-}rod} = H_{Trans\text{-}rod/Frit} - H_{Frit} = \omega_\beta^2 \omega_\lambda d_{Skel.} \quad (18)$$

where ω_β is the ratio of the differences between the extreme velocity across the rod diameter to the average velocity (u_S/ϵ_e) and $\omega_\lambda d_{Skel.}$ is the persistence-of-velocity length.

If we assume that the morphologies of the first and second generations of silica monolithic columns are self similar and the sizes of the porons and throughpores are decreased by the same factor of 1.6, we can reasonably assume that the flow streamlines merge and split at the same relative distances along the column, scaled to the domain size, 3.3 and 2.1 μm, respectively. The flow persistence length remains the same but it will take 1.6 times more flow exchange steps to reach it in the second than in the first generation of silica rods. In the previous work, based on the first generation of 4.6 mm I.D. silica monolithic columns, the persistence-flow-length, $\omega_\lambda d_{Skel.}$, was found equal to 2.2 cm for uracil (from the fit of the experimental trans-rod eddy diffusion term to the theoretical expression proposed by Giddings and a 3% relative velocity bias). Therefore, the relative velocity biases are estimated from Eq. (18) and $H_{Trans\text{-}rod} \simeq 8 - 3 = 5$ μm at $\omega_\beta = 1.5\%$. In conclusion, the radial velocity bias from the center to the wall of the 4.6 mm I.D. rod was nearly halved. The consequences are even more important since the trans-rod eddy diffusion term, which is proportional to the square of the relative velocity bias, is decreasing by a factor four.

4.2.5. Improvement in peak shape

In the previous section, we show evidence of the higher uniformity of the new silica rods prepared by Merck Millipore. From a qualitative viewpoint, the radial velocity bias taking place across these rods was been decreased to half what they were for the first generation of monolithic columns. Yet, a certain amount of bias remains.

The more radially homogeneous is a rod, the more symmetrical the peaks eluted from it. Fig. 7A and B compares the peak shapes of uracil (left graph) and naphthalene (right graph) eluted from columns of the first and the second generation of monolithic columns. The flow rate was high, at 3.0 mL/min. Whether the compound is retained or not, important peak tailings were observed with the columns commercialized in the early 2000s. Despite a longer residence time in the column and a larger diffusivity across the porons, the impact of the trans-column velocity biases, directly measured by Abia et al. [18,19] using electrochemical detection with a non-retained compound, tailing is still significant for naphthalene ($k \simeq 2.5$). This confirms that radial mixing was ineffective and that the time necessary for the exchange of the analyte molecules between the center and the wall regions of the rod was larger than or comparable to the retention time. In contrast, with a column having the same dimension but packed with superficially porous particles, 2.6 μm Kinetex-C_{18}, the trans-column velocity biases have no impact on the peak asymmetry because radial mixing is very effective in packed beds. So, the radial velocity biases seem to vanish for retained compounds as demonstrated in [60]. The column appears to be radially homogeneous and can deliver a high efficiencies. This scenario does not take place that easily in silica monolithic columns because radial mixing during the axial migration of the samples remains limited. It seems that the throughpores in monolithic columns behave as longitudinal channels, enhancing axial convection without much affecting radial eddy dispersion.

Slow radial mixing is a serious handicap for columns that are not radially homogeneous, which is the case of almost all types of LC columns today. The performance of monolithic columns can only be improved if radial velocity differences are minimized and if improved new frits and endfittings are developed. The actual frits used in Chromolith™ of first and second generations consist of six equidistant circular apertures, all located at about half the column radius from the column axis. This generates preferential flow directions for the in-going flow streamlets and obstructions for the out-going eluent streamlets leading to additional band broadening due to the sole presence of this type of frit. Standard frits distributing and collecting the eluent stream acroos the whole cross-section area of the silica rod would rather be preferred. Narrow columns have an advantage over conventional ones because diffusion proceed much faster over short distances but they present alternate difficulties. So, they may be preferred for some applications. Fig. 7A and B illustrates the impressive consequences of the development work undertaken to improve the quality of the Chromolith™ columns and their performance. We note a neat reduction of the peak tailing for naphthalene and uracil, in good agreement with

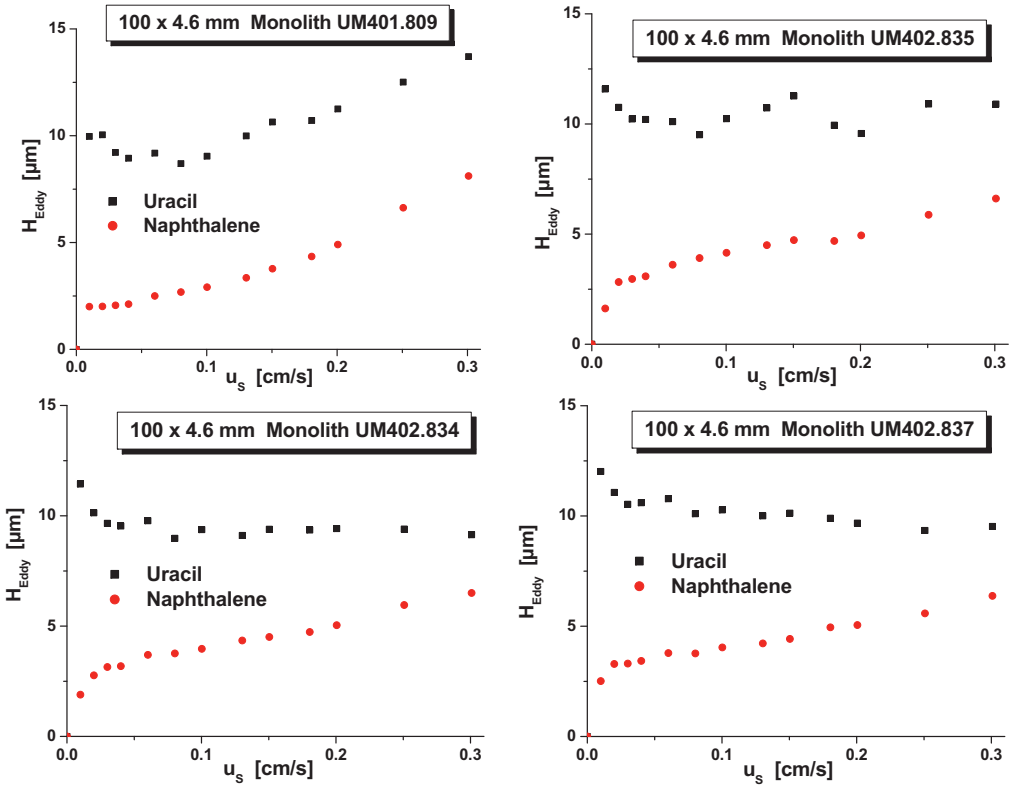

Fig. 6. Eddy diffusion of the four monolithic columns measured for a non-retained (uracil) and retained (naphthalene) compounds. There is a large difference between the two compounds.

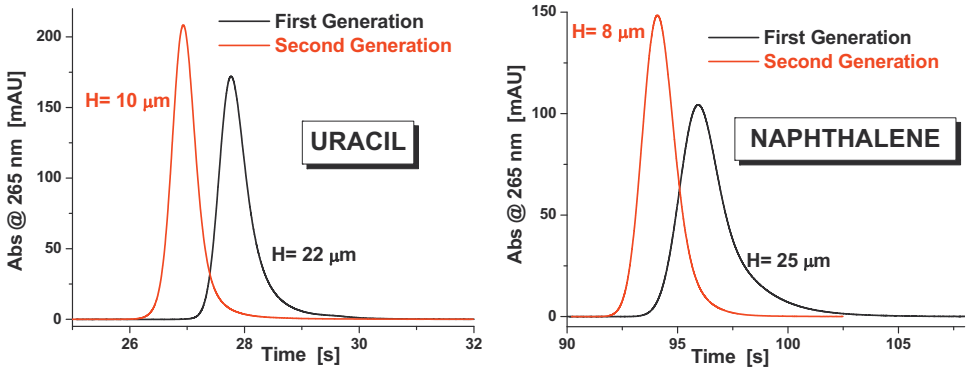

Fig. 7. Peak profiles recorded for a non-retained (left) and a retained (right) analytes on the first (solid black lines) and second (solid red lines) generation of monolithic columns provided by Merck. Note the improvement in peak symmetry (due to a 50% relative decrease of the trans-rod velocity bias) and the diminution of the half-height peak width (due to a 40% relative decrease of the domain size). (For interpretation of the references to color in this figure legend, the reader is referred to the web version of the article.)

the large diminution of the velocity bias across the rod diameter. The baseline peak width decreases then from 3 to 2.5 s for uracil and from 11 to 7.5 s for naphthalene. Also, the peak variance measured at half-height of the peak decreased by 40% which is consistent with the 37% decrease of the domain size. In conclusion, the second generation of Chromolith™ columns generate thinner and more symmetrical peaks than with the old first generation of columns.

5. Conclusion

The monolithic columns of the first generation provided elution peaks having unsymmetrical shape, hence relatively poor efficiencies, with a minimum HETP no smaller than 18 µm (as accurately measured from the peak variance [15]). These limitations were essentially due to a significant trans-column velocity biases (≃ 3% [30]). The new generation of these columns provides far more symmetrical elutions peaks. Using a protocol that involves the successive measurements of the longitudinal diffusion, the skeleton/liquid mass transfer resistance and the eddy diffusion terms, we were able to prove that the second generation of monolithic silica columns proposed by Merck Millipore may provide chromatograms with a three times higher efficiency (up to 155,000 plates/m, with a minimum HETP of 6.5 µm) than the first generation of these columns, which afforded only a maximum of 55,000 plates/m.

We found two important structural differences between the columns of the first and the second generation. First, the permeability measurements reveal a significant decrease of the domain size (sum of the average poron and throughpore sizes), from 3.3 to 2.1 µm (−35%). The direct consequence is a ca. 40% increase in the column efficiency (as measured from the half-height peak-width).

Secondly, the analysis of the eddy diffusion of a non-retained compound, obtained by subtraction of the trans-throughpore, the short-range inter-channel, and the frit/endfitting eddy diffusion contributions from the overall eddy diffusion term, shows that the trans-column relative velocity bias across the rod was reduced by 50% (down to $\simeq$ 1.5%). This means that more radially homogeneous silica rods can now be prepared. Because the symmetry of eluted peaks increases with increasing column radial homogeneity, the column efficiency (as accurately measured from the peak variance) increased by nearly 200%. However, the problem of the radial heterogeneity of monolithic rods has not yet been completely solved. Proof is provided by the HETP of a non-retained compound being higher at high flow rates than that of a moderately retained one. In contrast, somewhat less heterogeneous silica monoliths have been prepared by others, but these were narrower, shorter columns (2.3 mm × 50 mm and 3.2 mm × 50 mm). These columns provided smaller absolute efficiencies but plate counts close to 250,000/m, as determined following the same *modus operandi*.

The new monolithic columns provided by Merck Millipore have the permeability of columns packed with 4.5 μm spherical particles and the efficiency of columns packed with 3 μm conventional fully porous particles. Regrettably, however, the maximum inlet pressure under which they can be used does not exceed 200 bar because the silica rod must still be clad in a polyether ether ketone (PEEK) tube, which might break under higher pressures. Then, long Chromolith™ columns (25–50 cm) cannot be used safely if high plate counts (40,000–80,000 plates) and short analysis times (t_0< 10 s) are required. Under a 200 bar pressure, the hold-up time of the 10 cm long columns is 16 s and the superficial linear velocity of the eluent 5 mm/s (for a viscosity around 0.8 cP). A column of the same length, packed with sub-2 μm particles could provide a higher efficiency (250,000 plates/m) and has a smaller hold-up time t_0 = 9 s, when operated under 1200 bar [63]. Sub-3 μm core–shell particles can also generate higher efficiencies (200,000 plates/m) at higher speeds with t_0 = 8 s under 1000 bar [63]. The level of performance provided by the monolithic columns of the second generation provided by Merck Millipore is close to the one offered by columns packed with sub-2 μm fully porous and sub-3 μm superficially porous particles but they have not yet exceeded them. Their major advantage remains their higher permeability that allows their operation with low inlet pressures while their major drawback in this competition remains the impossibility to be operated beyond 200 bar. So far, this second generation of Chromolith™ columns is designed to provide an attractive permeability/efficiency alternative to conventional 400 bar instruments. We expect to see in a near future the preparation of a third generation of shorter and narrower monolithic columns to be operated safely at much higher pressures with the latest very high pressure instruments.

Nomenclature

List of symbols

B	longitudinal diffusion coefficient (m^2/s)
$C_{Skel.}$	trans-skeleton mass transfer coefficient (s)
d_{pore}	average mesopore size (m)
$d_{Throughpore}$	average throughpore size (m)
$d_{Skel.}$	average monolithic skeleton size (m)
D_{eff}	effective diffusion coefficient along the monolithic column (m^2/s)
$D_{Skel.}$	effective skeleton diffusivity (m^2/s)
D_m	bulk molecular diffusion coefficient (m^2/s)
F_v	flow rate (m^3/s)
H	total column HETP (m)
$H_{Throughpore}$	trans-throughpore eddy diffusion HETP term (m)
H_{Eddy}	eddy diffusion HETP term (m)
$H_{Long.}$	longitudinal diffusion HETP term (m)
H_{Short}	short-range inter-throughpore eddy diffusion HETP term (m)
$H_{Skel.}$	trans-skeleton mass transfer resistance HETP term (m)
$H_{Trans\text{-}rod/Frit}$	trans-rod and flow distribution/collection eddy diffusion HETP term (m)
$H_{Trans\text{-}rod}$	trans-rod eddy diffusion HETP term (m)
k	retention factor
k_1	zone retention factor
k_0	specific permeability (m^2)
K	Henry's equilibrium constant between the stationary and bulk phases
K_G	Ergun permeability constant
ΔP	pressure drop along the column (Pa)
R_c	column inner radius (m)
T	temperature during the HETP experiments (K)
Δt_p	variation of the parking residence time (s)
u_S	superficial linear velocity (m/s)
$u_{R,PP}$	migration linear velocity during the peak parking experiments (m/s)

Greek letters

ϵ_e	external column porosity
ϵ_t	total column porosity
ϵ_p	skeleton porosity
$\epsilon_{p,ref}$	reference skeleton porosity
γ_e	external obstruction factor
γ_p	internal obstruction factor
γ_p	reference internal obstruction factor
η	eluent viscosity (Pa s)
λ_m	ratio of the analyte size to that of the average mesopore size
$\lambda_{m,ref}$	reference ratio of the analyte size to that of the average mesopore size
ω_β	relative velocity bias from the center to the wall of the silica rod
ω_λ	relative persistence-of-flow length
Ω	ratio of the sample diffusivity in the porons to the bulk molecular diffusion coefficient
$\Delta\sigma^2_{PP}$	increment of the peak variance in the parking method experiments (s^2)

Acknowledgements

This work was supported in part by the cooperative agreement between the University of Tennessee and the Oak Ridge National Laboratory. We thank Karin Cabrera (Merck Millipore, Darmstadt, Germany) for the generous gift of the new prototypes of monolithic columns.

References

[1] K. Nakanishi, N. Soga, J. Am. Ceram. Soc. 74 (1991) 2518.
[2] H. Minakuchi, K. Nakanishi, N. Soga, N. Ishizuka, N. Tanaka, Anal. Chem. 68 (1996) 3498.
[3] H. Minakuchi, K. Nakanishi, N. Soga, N. Ishizuka, N. Tanaka, J. Chromatogr. A 797 (1998) 121.
[4] K. Cabrera, G. Wieland, D. Lubda, K. Nakanishi, N. Soga, H. Minakuchi, K. Unger, Trends Anal. Chem. 17 (1998) 133.
[5] S. Hjerten, J.-L. Liao, J. Chromatogr. 457 (1988) 165.
[6] F. Svec, J. Frechet, Anal. Chem. 64 (1992) 820.
[7] Q. Wang, F. Svec, J. Frechet, J. Chromatogr. A 669 (1994) 230.
[8] M. Kele, G. Guiochon, J. Chromatogr. A 960 (2002) 19.
[9] K. Miyabe, G. Guiochon, J. Phys. Chem. B 106 (2002) 8898.
[10] F. Gritti, W. Piatkowski, G. Guiochon, J. Chromatogr. A 983 (2003) 51.
[11] F. Gritti, W. Piatkowski, G. Guiochon, J. Chromatogr. A 978 (2002) 81.
[12] F. Gritti, G. Guiochon, J. Chromatogr. A 1028 (2004) 105.
[13] K. Cabrera, J. Sep. Sci. 27 (2004) 843.
[14] G. Guiochon, J. Chromatogr. A 1168 (2007) 101.
[15] F. Gritti, G. Guiochon, J. Chromatogr. A 1218 (2011) 4452.

[16] P. Stevenson, F. Gritti, G. Guiochon, J. Chromatogr. A 1218 (2011) 8255.
[17] 31st International Symposium on High Performance Liquid Phase Separations and Related Techniques (HPLC-2007), Ghent, Belgium.
[18] K.S. Mriziq, J.A. Abia, Y. Lee, G. Guiochon, J. Chromatogr. A 1193 (2008) 97.
[19] J. Abia, K. Mriziq, G. Guiochon, J. Chromatogr. A 1216 (2009) 3185.
[20] J.R. Mazzeo, U.D. Neue, M. Kele, R.S. Plumb, Anal. Chem. 77 (2005) 460A.
[21] J.J. Kirkland, T.J. Langlois, J.J. DeStefano, Am. Lab. 39 (2007) 18.
[22] J.J. DeStefano, T.J. Langlois, J.J. Kirkland, J. Chromatogr. Sci. 46 (2008) 254.
[23] F. Gritti, G. Guiochon, J. Chromatogr. A 1157 (2007) 289.
[24] F. Gritti, I. Leonardis, D. Shock, P. Stevenson, A. Shalliker, G. Guiochon, J. Chromatogr. A 1217 (2010) 1589.
[25] G. Guiochon, F. Gritti, J. Chromatogr. A 1218 (2011) 1915.
[26] C. Horváth, S.R. Lipsky, J. Chromatogr. Sci. 7 (1969) 109.
[27] C.G. Horváth, B.A. Preiss, S.R. Lipsky, Anal. Chem. 39 (1967) 1422.
[28] J.J. Kirkland, Anal. Chem. 41 (1969) 218.
[29] J.J. Kirkland, Anal. Chem. 64 (1992) 1239.
[30] F. Gritti, G. Guiochon, J. Chromatogr. A 1218 (2011) 5216.
[31] D. Hlushkou, S. Bruns, A. Holtzel, U. Tallarek, Anal. Chem. 82 (2010) 7150.
[32] D. Hlushkou, S. Bruns, U. Tallarek, J. Chromatogr. A 1217 (2010) 3674.
[33] S. Bruns, T. Hara, B. Smarsly, U. Tallarek, J. Chromatogr. A 1218 (2011) 5187.
[34] F. Gritti, G. Guiochon, J. Chromatogr A, doi:10.1016/j.chroma.2011.12.065, in press.
[35] F. Gritti, G. Guiochon, Chem. Eng. Sci. 65 (2010) 6327.
[36] F. Gritti, G. Guiochon, J. Chromatogr A 1221 (2012) 2–40.
[37] F. Gritti, G. Guiochon, J. Chromatogr. A 1217 (2010) 907.
[38] F. Gritti, G. Guiochon, J. Chromatogr. A 1217 (2010) 8167.
[39] F. Gritti, J. Omamogho, G. Guiochon, J. Chromatogr. A 1218 (2011) 7078.
[40] F. Gritti, G. Guiochon, J. Chromatogr. A 1169 (2007) 125.
[41] J. Knox, H. Scott, J. Chromatogr. 282 (1983) 297.
[42] F. Gritti, G. Guiochon, Chem. Eng. Sci. 61 (2006) 7636.
[43] K. Miyabe, Y. Matsumoto, G. Guiochon, Anal. Chem. 79 (2007) 1970.
[44] F. Gritti, G. Guiochon, J. Chromatogr. A 1218 (2011) 3476.
[45] F. Gritti, G. Guiochon, Chem. Eng. Sci. 66 (2011) 3773.
[46] J. Giddings, Dynamics of Chromatography, Marcel Dekker, New York, NY, 1965.
[47] F. Gritti, G. Guiochon, J. Chromatogr. A 1217 (2010) 5137.
[48] S. Ergun, Chem. Eng. Prog. 48 (1952) 89.
[49] F. Gritti, G. Guiochon, AIChE J. 57 (2011) 346.
[50] F. Gritti, G. Guiochon, AIChE J. 57 (2011) 333.
[51] F. Gritti, G. Guiochon, J. Chromatogr. A 1218 (2011) 8209.
[52] H. Gao, P. Stevenson, F. Gritti, G. Guiochon, J. Chromatogr. A 1222 (2012) 81–89.
[53] J.H. Knox, L. McLaren, Anal. Chem. 36 (1964) 1477.
[54] K. Miyabe, N. Ando, G. Guiochon, J. Chromatogr. A 1216 (2009) 4377.
[55] Y. Miyabe, K. Matsumoto, G. Guiochon, Anal. Chem. 65 (2010) 3859.
[56] L. Pismen, Chem. Eng. Sci. 29 (1974) 1227.
[57] E. Renkin, J. Gen. Physiol. 38 (1954) 225.
[58] F.M.C.A. Mitzithras, J.H. Strange, J. Mol. Liq. 260 (1992) 273.
[59] F. Gritti, G. Guiochon, AIChE J. 56 (2010) 1495.
[60] F. Gritti, G. Guiochon, J. Chromatogr. A 1217 (2010) 6350.
[61] F. Gritti, G. Guiochon, Anal. Chem. 5329 (2006) 78.
[62] D. Hlushkou, S. Bruns, A. Seidel-Morgenstern, U. Tallarek, J. Sep. Sci. 34 (2011) 2026.
[63] F. Gritti, G. Guiochon, J. Chromatogr A, doi:10.1016/j.chroma.2011.07.014.